Macromolecular Research, Vol. 25, No. 3, pp 231-242 (2017)
DOI 10.1007/s13233-017-5032-x

www.springer.com/13233
pISSN 1598-5032 eISSN 2092-7673

Phase Separation and Electrical Conductivity of Nanocomposites Made of Ether-/Ester-based Polyurethane Blends and Carbon Nanotubes

Minho Lee[1], Jahun Koo[1], Hoil Ki[1], Kyung Hoon Lee[1], Byong Hun Min[1], Young Chul Lee[2], and Jeong Ho Kim*[,1]

[1]Department of Chemical Engineering, University of Suwon, Gyeonggi 18323, Korea
[2]Green process and Materials R&D Group, Korea Institute of Industrial Technology, Chungnam 31056, Korea

Received August 16, 2016; Revised November 18, 2016; Accepted December 4, 2016

Abstract: Nanocomposites made of blends of ether-based thermoplastic polyurethanes (TPUs) and ester-based TPUs with multi-walled carbon nanotubes (MWCNTs) were studied. The TPU blend/MWCNT nanocomposites had higher electrical conductivities than those containing a single TPU. At a specific MWCNT loading, quenched or annealed TPU blend nanocomposites exhibited electrical conductivities three to four orders of magnitude larger than single TPU samples. Using Lorentz corrections, invariant quantity, Q_{inv}, in small-angle X-ray scattering (SAXS) analysis, MWCNTs were found to retard phase separation. Raman spectra indicated the existence of interactions between phenyl rings in the TPUs and the MWCNT. Good dispersion of MWCNTs in the TPU blend was observed with transmission electron microscopy (TEM); both isolated droplet and co-continuous phase-separated morphologies were shown. Fourier transform infrared spectroscopy (FTIR) analysis and differential scanning calorimetry (DSC) measurements were performed to investigate the changes in morphology. Dynamic mechanical analysis (DMA) results were consistent with the DSC results.

Keywords: nanocomposite, multi-walled carbon nanotube, blend, thermoplastic polyurethane, phase separation.

Introduction

Polyurethanes are synthesized usually by reacting hydroxyl terminated ethers or esters with isocyanate compounds. Most of resulting polyurethanes are thermosetting but thermoplastic polyurethanes (TPUs) are also made due to their versatility in processing. TPUs can be synthesized using diols. They are used in a variety of industrial applications such as automotive, electronics, painting and coating, adhesives, *etc*.[1,2] They are recently used in some specialty areas such as in the biomedical and tissue engineering.[3] TPUs are segmented polymers composed of hard and soft segments forming a two-phase microstructure. The hard segment is formed by extending a diisocyanate with a chain extender, whereas the soft segment is formed from linear, long-chain hydroxyl-terminated polyols. In TPUs, phase separation of the hard and soft segments into micro domains is observed even when the segment length is relatively short, owing to the thermodynamic incompatibility between the polar hard and non-polar soft segments. The micro-phase separation of hard and soft segments in TPUs has been shown by small-angle X-ray scattering (SAXS),[4] differential scanning calorimetry (DSC),[5] and transmission electron microscopy (TEM).[6] Another driving force for domain formation is the strong intermolecular interaction between urethane units, which are capable of forming inter-urethane hydrogen bonds.[7]

Considerable efforts have been devoted to conductive polymer nanocomposites in view of electronic applications such as electrostatic discharge dissipation, electromagnetic interference shielding, charge-storage, *etc*.[8-13] As conductive carbonaceous fillers, carbon blacks, carbon fibers or carbon nanotubes can be used.[14-18] Multi-walled carbon nanotubes (MWCNTs) exhibit extraordinary mechanical, electrical, thermal, and optical properties, which make them highly interesting for applications in materials science.[19-27] In recent years, polymer/MWCNT nanocomposites have been extensively studied, specifically with regard to the interfacial phenomena between MWCNTs and polymers, with the goal of achieving better properties than can be obtained with conventional composites. In polymer/MWCNT nanocomposites, the interaction between the matrix polymers and the MWCNTs plays an important role in determining the state of the MWCNT dispersion. Nanocomposites of polymer blends with MWCNTs are more complicated than those of single polymers and MWCNTs because in some cases, the percolation threshold values of the polymer blend/MWCNT nanocomposites can be reduced, whereas that of single polymer/MWCNT nanocomposites cannot.[28,29] Very low percolation threshold value was reported in the blend of polycarbonate and polyethylene with MWCNTs.[30,31] The co-continuous morphology exhibiting double percolation behavior was attributed to this low threshold value. Improve-

*Corresponding Author. E-mail: jhkim@suwon.ac.kr

ment of mechanical and electrical properties of CNT filled PET/PVDF blend was also reported to be due to selective localization of MWCNT in PET phase.[32] A co-continuous structure and lower electrical percolation threshold were observed in polypropylene/ABS blends with MWCNTs.[33] Selective location and double percolation of carbon fiber were also reported in short carbon fiber filled HDPE/polypropylene blends.[15] Decrease in percolation threshold in these blends can be understood in terms of percolation theory where formation of connected network of conductive fillers is the key issue for electrical conductivity of polymeric nanocomposites.[8,9,34,35]

TPU containing carbonaceous fillers have been reported in the literature.[14,19-21,36,37] Very low percolation threshold value was observed in TPU/MWCNT nanocomposites.[19] Improvement in tensile properties in TPU nanocomposites by adding MWCNT was also reported.[20] Though single TPU/MWCNT nanocomposites were widely studied, nanocomposites of TPU blends with MWCNTs have not been extensively explored. TPU/polypropylene blend containing carbon black fillers was reported in the literauture.[14] TPUs synthesized from mixtures of ether- and ester-polyols were reported to show unique elastomeric properties such as excellent mechanical properties and weatherability.[38] Instead of synthesizing mixed polyol TPUs, ether TPUs and ester TPUs can be mixed together into blends to give tailored properties depending on the composition of the two TPUs.

In this study, nanocomposites of blends of ether-based and ester-based TPUs, denoted herein as ether-TPU and ester-TPU, respectively, with MWCNTs are investigated. The aim of our study is to present the effect of MWCNT on the morphology and the physical properties of nanocomposites including electrical conductivity of the TPU blend/MWCNT nanocomposites. Since TPU blend /MWCNT nanocomposites were prepared by melt processing in a twin-screw extruder, the effect of thermal treatment, *i.e*., quenching or annealing after melt blending, was also studied. Electrical conductivity measurements, transmission electron microscopy (TEM) and small-angle X-ray scattering (SAXS) analyses, Fourier transform infrared spectroscopy (FTIR), and dynamic mechanical analysis (DMA) were conducted to characterize the state of MWCNT dispersion in the polymer blend matrix and its influence on the morphology and physical properties of the nanocomposites.

Experimental

Materials. Two types of TPUs were obtained from SK Chemicals (Korea): polyether-based TPU (Skythane R185A, M_w=250,000) and polyester-based TPU (Skythane S185A, M_w=250,000). Both types of TPUs have similar Shore hardness values of 87A. The hard segments of both the ether-based and ester-based TPUs are made of 4,4-diphenylmethane diisocyanate (MDI) and 1,4-butanediol (BD), but the soft segments are different: the ether type contains poly(tetramethylene oxide) glycol (PTMG, M_w=1,000), whereas the ester type contains poly(butylene adipate) glycol (PBAG, M_w=1,000).

Thin MWCNTs (NC7000), synthesized by catalytic chemical vapor deposition (CCVD) and having a purity of approximately 90 wt% (Nanocyl Company, Belgium) were used for the preparation of the nanocomposites. The average diameter, length, and surface area of the MWCNTs were 9.5 nm, 1.5 μm, and 250-300 m^2/g, respectively. The MWCNTs were used as obtained without further purification.

Preparation of TPU/MWCNT Nanocomposites. TPU pellets were dried for 4 h prior to melt blending and MWCNTs were dried in a vacuum oven at 80 °C for 12 h. Then, all the components were melt blended in an extruder. The MWCNT loadings in all the nanocomposite samples were set to be 0, 0.5, 1.0, 1.5, and 2.0 wt%. TPUs and MWCNTs were fed into the extruder simultaneously and melt mixing was carried out in a twin-screw extruder (BA-19ST, Bautek Corp., Korea). The nanocomposites were processed at temperatures in the range of 170-185 °C depending on their position in the extruder. The extrudates were pelletized and subjected to hot-press molding at 185 °C for 5 min under a pressure of 5.0 MPa to obtain thin-film specimens. The dimensions of the nanocomposite samples were 10 cm × 10 cm, with a thickness of approximately 0.4 mm.

After hot pressing, two types of sample preparation methods, annealing and quenching, were used to investigate the effect of the thermal treatment on the properties of the nanocomposites. For quenching, the thin-film specimens were quickly quenched in liquid nitrogen. For annealing, the nanocomposite specimens were annealed at 100 °C in an oven for 72 h and quickly quenched in liquid nitrogen.

Sample designation will be used hereinafter as follows: the first capital letter before TPU denotes the polyurethane type, followed by one or two letters in the parenthesis: the first letter "C" exhibits the 1 wt% of MWCNT in the sample and the second letter "A or Q" shows the thermal treatment method, respectively. For instance, T-TPU (Q) denotes a quenched sample containing ether-based polyurethane without MWCNTs and S-TPU (C/A) refers to an annealed nanocomposite with ester-based polyurethane with 1.0 wt% MWCNT. The nanocomposites containing blends of ether-TPU and ester-TPU were designated by using "B" as the first capital letter to denote a blend. For example, B-TPU (C/A) denotes an annealed sample containing 50 wt% ether-TPU and 50 wt% ester-TPU with 1.0 wt% MWCNT. Samples, thus, prepared were listed in Table I.

Characterization and Measurement. To check the electrical conductivity of samples, electrical volume resistivity which is the reciprocal of electrical conductivity was measured using a multi-meter (Protek 608, GS Instrument, Korea) at 2.5 V with a two-point probe.

TEM images of the nanocomposite specimens were obtained at the Korea Basic Science Institute in the energy filtering mode (EM-912 Omega, Carl Zeiss Co., Germany) at an operating voltage of 120 kV. The ultrathin sectioning was performed

Table I. Sample Designation of TPU/MWCNT Nanocomposites

Polymer and MWCNT Composition (wt%)			Sample Designation	
Ether-TPU (T-TPU)	Ester-TPU (S-TPU)	MWCNT (C)	Samples Prepared from Quenching (Q)	Samples Prepared from Annealing (A)
100		-	T-TPU (Q)	T-TPU (A)
	100	-	S-TPU (Q)	S-TPU (A)
50	50	-	B-TPU (Q)	B-TPU (A)
99		1	T-TPU (C/Q)	T-TPU (C/A)
	99	1	S-TPU (C/Q)	S-TPU (C/A)
49.5	49.5	1	B-TPU (C/Q)	B-TPU (C/A)

on an ultra-microtome at -100 ºC.

Raman spectroscopy (T64000, HORIABA Jobin Yvon, France) was done using a 514 nm Ar laser and 80 mW laser power to investigate the interactions between the MWCNTs and the polymer in the nanocomposites. The resolution and wavelength range of the lasers were 0.6 cm^{-1} and 1000-2000 cm^{-1}, respectively.

SAXS (SAXSess MC2 with SAXSquant 3.x software, Anton Paar, Austria) experiments were carried out with a sealed X-ray tube ($\lambda_{Cu(K\alpha)}$=0.1542 nm). The X-ray beam was generated at 40 kV and 50 mA of power. The samples (thickness: 0.4 mm) were introduced into a paste cell and placed in an evacuated chamber. The sample-to-detector distance was 50 cm. Each SAXS pattern corresponded to a data collection time of 600 s. The scattering data obtained for each sample as a function of q (scattering vector) are denoted by $q=(4\pi/\lambda)\sin\theta$, where λ is the X-ray wavelength and θ is the scattering angle.

FTIR (FTIR-4200, Jasco, Japan) was performed by the attenuated total reflection (ATR) mode at a resolution of 4 cm^{-1}. The thermal properties of the nanocomposites were measured by DSC (Q20, TA Instruments, USA) at a heating rate 20 ºC/min in nitrogen atmosphere after annealing and quenching. It was conducted by heating the samples from -150 to 250 ºC during which thermograms were taken for first-run analysis.

DMA was performed using a dynamic mechanical analyzer (SS6100, Seiko Instrument Inc., Japan) at an amplitude of 4.5 μm and a frequency of 1 Hz in nitrogen atmosphere. The temperature was increased at a rate of 20 ºC/min over the temperature range from -100 to 160 ºC.

Results and Discussion

Electrical Resistivity of TPU/MWCNT Nanocomposites. Figure 1 shows the electrical volume resistivity of TPU/MWCNT nanocomposites prepared by quenching or annealing after hot pressing. The electrical conductivity measurements can be affected by the location of the contact regions in the same sample as well as the contact resistance. To account for these, several measurements were done and results are shown with error bars in Figure 1.

As the MWCNT loading increased, the electrical resistivity decreased in both the quenched and annealed samples. The quenched samples of the TPU blend/MWCNT nanocomposites showed lower electrical resistivity than either the ether- or ester-based TPU/MWCNT nanocomposites at MWCNT loadings above 1.0 wt%, as shown in Figure 1(a). This is quite an interesting result which is often observed in the phase separated blend nanocomposites containing conductive fill-

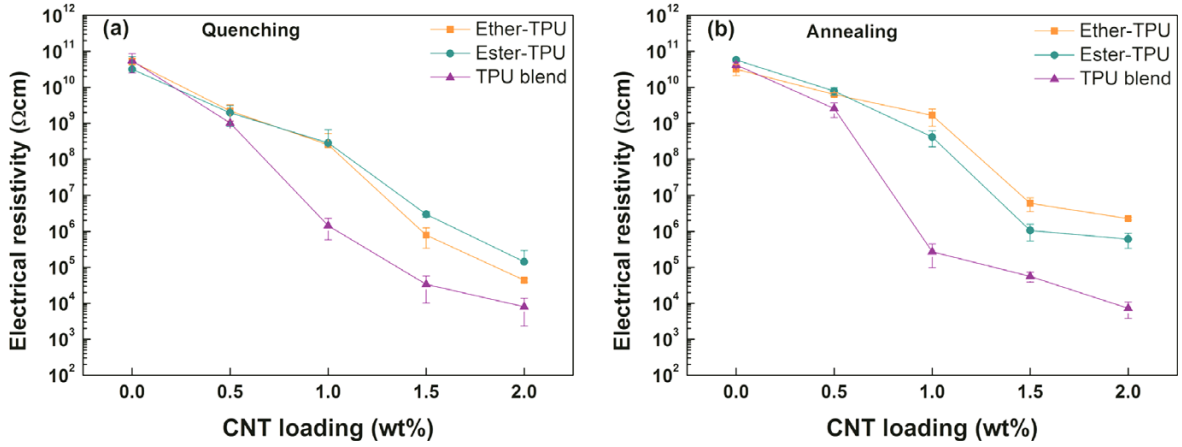

Figure 1. Electrical volume resistivity of TPU/MWCNT nanocomposites as a function of MWCNT loading prepared by different thermal treatment: (a) quenching and (b) annealing.

ers.[30,31] This is explained in terms of double percolation and selective localization of conductive fillers in the literature. It is noted that at 1.0 wt% loading, the quenched TPU blend nanocomposites exhibited electrical volume resistivities around three orders of magnitude smaller than single TPU nanocomposites.

The annealed TPU blend/MWCNT nanocomposites also showed lower electrical resistivity than either the ether- or ester-based TPU/MWCNT nanocomposites at MWCNT loadings above 1.0 wt%, as shown in Figure 1(b). Similar result is shown in these annealed samples as for quenched nanocomposites such that at 1.0 wt% loading, the annealed TPU blend nanocomposites exhibited electrical volume resistivities around four orders of magnitude smaller than single TPU nanocomposites.

Electrical conductivity of polymeric nanocomposites can be explained in terms of percolation theory. At the percolation threshold, a connected network of conductive fillers is formed through which the electrons can move imparting electrical conductivity to nanocomposites.[8,9,34,35] Accordingly, the morphology in the TPU blend/MWCNT nanocomposite becomes an important factor affecting the electrical volume resistivity. Electrical conductivity of the nanocomposites depend on many factors such as filler content, inherent conductivity, size and aspect ratio of fillers, intrinsic properties of polymer matrix, the quality of interaction between conductive fill and polymer matrix, dispersion state of filler, mixing technique, crystallinity of the polymer matrix, *etc*.[8,9] Since the morphology including state of MWCNT dispersion appears to be a very important factor determining the electrical resistivity in this study, the effect of MWCNT on the morphology was investigated. The phase separation behavior of the TPU blend/MWCNT nanocomposites may give rise to different morphologies for the quenched and annealed samples. In studying the nanocomposites, the difficulty was that no single characterization technique could adequately describe the state of MWCNT dispersion and phase behavior in the composite; combined characterization methods were necessary and thus TEM, Raman spectroscopy, and SAXS analyses were carried out. To observe visually the level of dispersion of the MWCNTs and the phase separation in the polymer matrix, TEM images of the samples were acquired and the results are discussed in the following section. Raman spectroscopy and SAXS results are then presented to support the TEM analysis.

TEM Results. TEM images of ether-TPU/MWCNT nanocomposites containing 1.0 wt% MWCNT prepared by quenching and annealing are shown in Figures 2(a) and (b), respectively. The MWCNTs in the figures show fair dispersion in the polyurethane matrix, with some agglomerates of MWCNTs in some areas. This observation is in agreement with our previous electrical resistivity, in which single TPU/MWCNT nanocomposites exhibited fair electrical volume resistivity. TEM images of the ester-TPU/MWCNT nanocomposites containing 1.0 wt% MWCNT prepared by quenching and annealing are shown in Figures 2(c) and (d), respectively. Similar MWCNT dispersion as the ether- TPU/MWCNT nanocomposites was observed.

Figures 2(e) and (f) are images for quenched and annealed TPU blend/MWCNT nanocomposites, respectively. The MWCNTs showed relatively good dispersion especially in the annealed TPU blend/MWCNT nanocomposites in Figure 2(f) such that many thin long MWCNT tubes are seen.

In the quenched TPU blend/MWCNT nanocomposites in Figure 2(e) (higher magnification image as an inset), most of the MWCNTs were located along the dark areas. Since the bright areas are ether-TPUs and the dark areas are ester-TPUs, the MWCNTs are observed to reside mainly in the ester-TPU phase. The percolation threshold values of the phase-separated polymer blend/MWCNT nanocomposites were reported in a previous study to have decreased as compared to those of single-component polymer/MWCNT nanocomposites when MWCNTs are preferentially located in one phase of phase-separated blend nanocomposites.[39] Similar reasoning may be applied to the quenched TPU blend/MWCNT nanocomposites such that selective localization of MWCNT in the ester-TPU phase may help form conductive paths, contributing to the low electrical volume resistivity of the TPU blend/MWCNT nanocomposites.

In the annealed TPU blend/MWCNT nanocomposite, more interfacial areas were observed owing to the finer phase-separated morphology and the MWCNTs were very well dispersed, as shown in Figure 2(f).

TEM images of the TPU blend without MWCNTs prepared by quenching and annealing are shown in Figure 3(a) and (b), respectively. In these images, the bright areas are ether-TPUs and the dark areas are ester-TPUs. In the TPU blend, there was some degree of incompatibility between the polyether soft segment of the ether-TPU and polyester soft segment of the ester-TPU, resulting in phase separation between ether-TPU and ester-TPU.

As seen in Figure 3(a), B-TPU (Q) shows a phase-separated morphology similar to nucleation and growth (NG) with isolated droplet-shaped domains, whereas B-TPU (A) shows a co-continuous phase-separated morphology similar to spinodal decomposition (SD), as shown in Figure 3(b). SD-type phase separation is known to occur in unstable regions in the phase diagram, whereas NG-type phase separation occurs in the metastable region.[40] The TEM results in Figure 3 show that the TPU blend is in the metastable region at the melt mixing temperature, whereas it is in the unstable region at the annealing temperature.

A poly(ethylene glycol) (PEG)/poly(ε-caprolactone) (PCL) blend was reported in the literature to have an upper critical solution temperature (UCST), meaning that the miscibility increased with increasing temperature.[41] Since the structures of PEG and PCL resemble the structures of polyols of ether-TPUs and ester-TPUs respectively, ether-TPUs and ester-TPUs are thought to have similar behavior with changes in tempera-

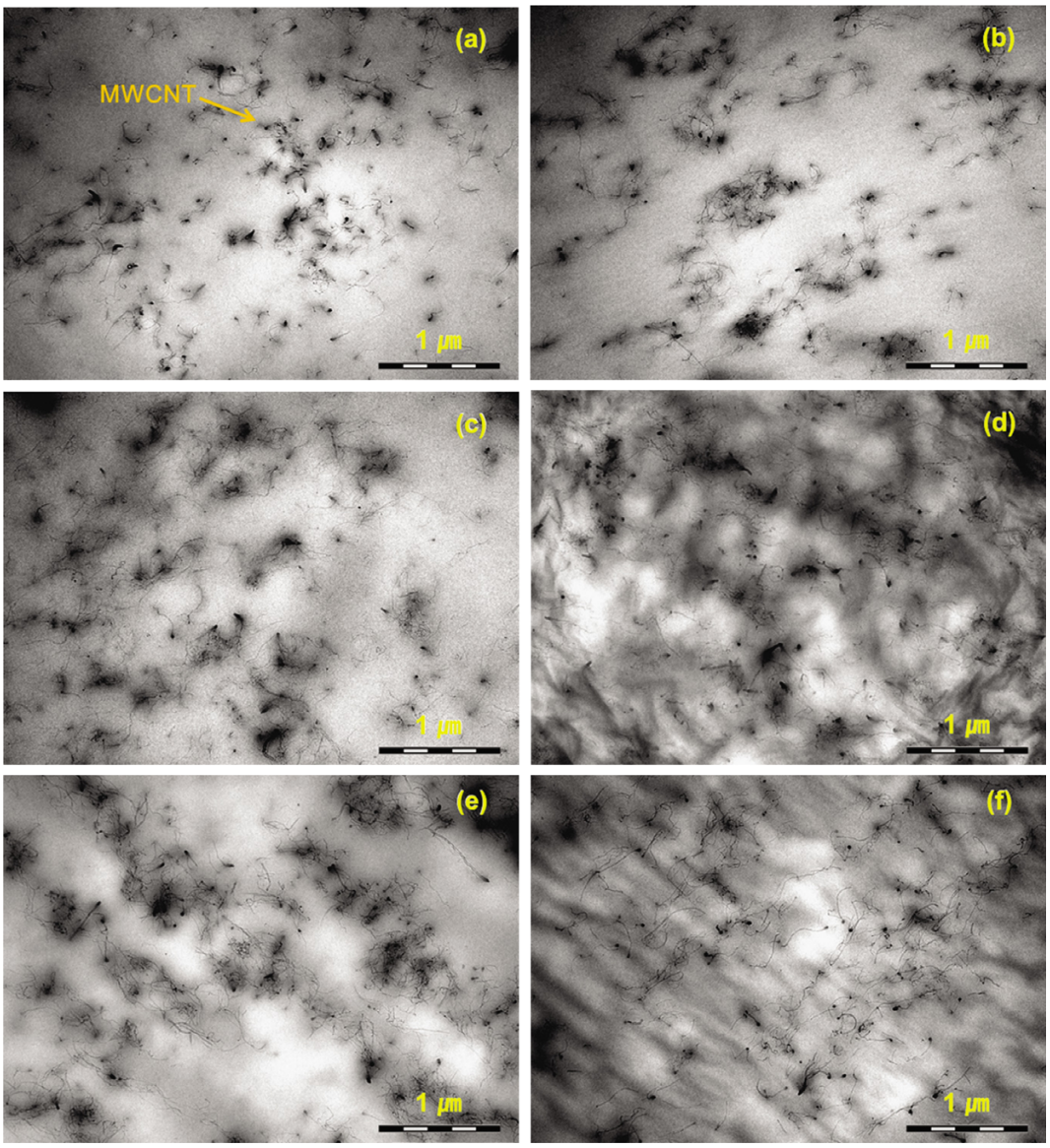

Figure 2. TEM images of TPU/MWCNT nanocomposites prepared by different thermal treatment; (a) T-TPU (C/Q), (b) T-TPU (C/A), (c) S-TPU (C/Q), (d) S-TPU (C/A), (e) B-TPU (C/Q), and (f) B-TPU (C/A).

ture. At the melt temperature which is higher than the annealing temperature, TPU blends are thought to be in the metastable region. By annealing it at a lower temperature, The B-TPU (A) sample is thought to be taken into the unstable region resulting in a SD-type morphology. This may explain the morphology shown in Figure 3.

Figures 3(c) and (d) show TEM images of the TPU blend/MWCNT nanocomposite containing ether- and ester-TPUs (50/50) with 1.0 wt% MWCNT prepared by quenching and annealing, respectively. Comparison between TPU blends without MWCNT (Figure 3(b)) and those with MWCNT (Figure 3(d)) in annealed samples exhibit some differences in morphology. Blends without MWCNT show coarse co-continuous structure while TPU blends with MWCNT show finer co-continuous phase separated structure resulting in more phase boundaries than TPU blends without MWCNT. Since fine co-continuous structure grows to coarse co-continuous structure during SD-type phase separation, this indicates that MWCNT retarded phase separation in TPU blends. Comparing the quenched TPU blend without MWCNT (Figure 3(a)) and those with MWCNT (Figure 3(c)), phase separation appears to be also retarded by the presence of MWCNT in these quenched samples since the droplet- type domains are not seen in Figure 3(c). The above-mentioned morphologies are consistent with the lower electrical volume resistivity of the annealed TPU blend/MWCNT nanocomposites as compared with the quenched samples, as exhibited in Figure 1. From these TEM results, MWCNTs are thought to reduce the phase separation. During nanocom-

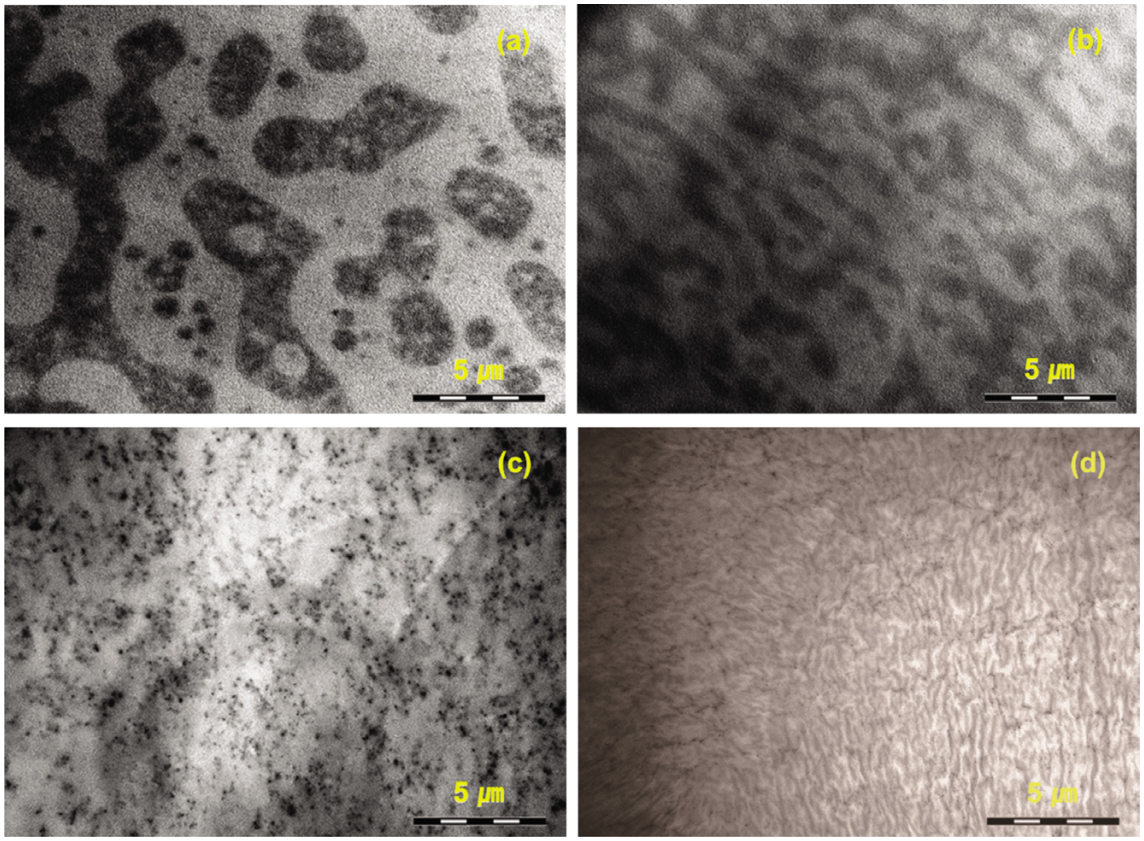

Figure 3. TEM images of TPU blend and TPU blend/MWCNT nanocomposites prepared by different thermal treatment: (a) B-TPU (Q), (b) B-TPU (A), (c) B-TPU (C/Q), and (d) B-TPU (C/A).

posite preparation, good dispersion of MWCNTs in the TPU blend/MWCNT nanocomposites may retard the phase separation not only due to some interaction between MWCNTs and blend TPUs but also due to the increase in matrix viscosity. To investigate if there exists some interaction between MWCNT and ether- or ester-TPU, Raman spectroscopy was applied to TPU blends.

Raman Spectroscopy. Figures 4(a) and (b) show the Raman spectra of neat MWCNTs and TPU/MWCNT nanocomposites containing 1.0 wt% MWCNT prepared by quenching and annealing, respectively. The broad band around 1584 cm^{-1} in the neat MWCNTs is referred to as the G-band, which is known to arise from the stretching of C-C bond in the graphitic materials.[42-44]

In the spectra of the TPU/MWCNT nanocomposites, the band at approximately 1618 cm^{-1} appears with a small shoulder at approximately 1600 cm^{-1}. The 1618 cm^{-1} peak may be assigned to be the vibrational mode for the aromatic ring in phenylene groups of MDI as 1612 cm^{-1} was reported to be the absorption peak of the phenylene group in the literature.[45]

If the 1618 cm^{-1} band with a shoulder is resolved into two bands, the peak position of the shoulder band at approximately 1600 cm^{-1} can be identified. This shoulder peak can be regarded as either some of phenylene groups having different morphology from those at 1618 cm^{-1} band due to the interaction with MWCNTs or the G-band of MWCNTs shifted from the 1584 cm^{-1} of the neat MWCNTs.

In Figure 4(a), the positions of the shoulder band for the quenched ether-TPUs, ester-TPUs, and TPU blend/MWCNT nanocomposites are estimated to be 1598, 1605, and 1608 cm^{-1}, respectively. In Figure 4(b), the corresponding positions for the annealed samples are 1597, 1605, and 1611 cm^{-1}, respectively. This appearance of the shoulder band indicates the existence of the interaction between phenylene groups of TPUs and the MWCNTs in all TPU/MWCNT nanocomposites since no such shoulder is observed for TPU blends without any MWCNTs as shown in Figure 4. This interaction may result from π-π stacking of phenyl rings in TPU hard segments and MWCNTs. Shifts in G-bands in Raman spectra were reported to be a manifestation of this kind of interaction in a previous study.[46]

SAXS Analysis. As mentioned above, the addition of MWCNTs in TPU blend/MWCNT nanocomposites decreased the extent of phase separation in the TPU blend. SAXS proved to be quite effective in the blend study because the SAXS technique can provide information on macro- and micro-phase separation in polymer blends.[47]

The SAXS patterns acquired for the ether- and ester-TPU/

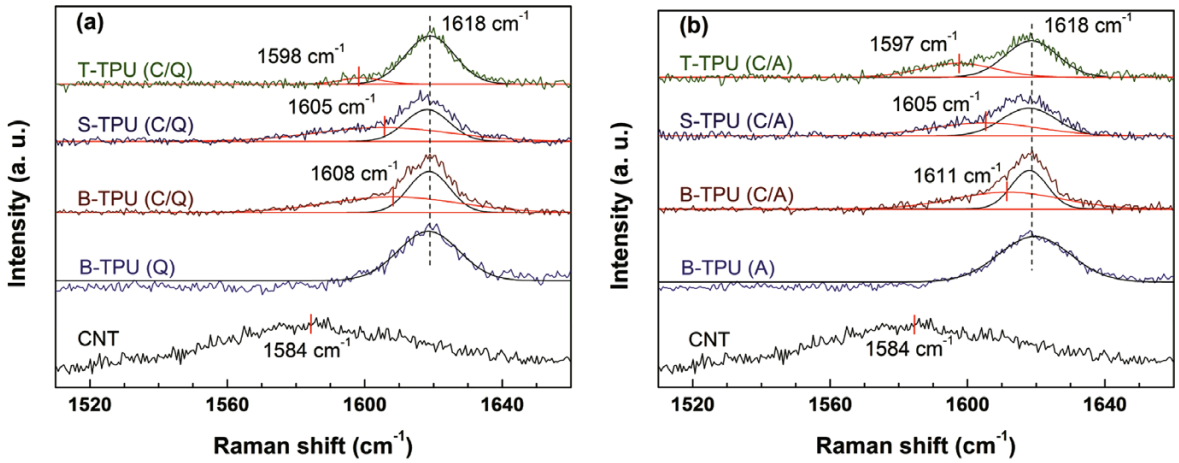

Figure 4. Raman spectra of TPU/MWCNT nanocomposites prepared by different thermal treatment: (a) quenching and (b) annealing.

MWCNT and TPU blend/MWCNT nanocomposites are shown in Figures 5(a)-(c), respectively. Here, $I_{(q)}$ is the X-ray scattering intensity and q is the scattering vector such that $q=(4\pi/\lambda)\sin\theta$ where λ and θ are the wavelength of the X-ray and the scattering angle, respectively. In Figure 5(a), a maximum in the scattering profile is observed at $q\approx0.2$ nm in both the ether-TPUs and ether-TPU/MWCNT nanocomposites. Since the presence of scattering peaks is usually interpreted as a consequence of the presence of distinct micro-phases with different electron densities, a maximum in the ether-TPU/MWCNT nanocomposites or in ether-TPUs indicates micro-phase- separated structures in these samples. The scattering intensity of the ether-TPU/MWCNT nanocomposites is observed to be higher than that of ether-TPUs without MWCNTs. Also, the scattering intensities of the annealed ether-TPU/MWCNT nanocomposites and annealed ether-TPUs are observed to be higher than those of the quenched ether-TPU/MWCNT nanocomposites and quenched ether-TPUs.

Similar trends are observed for the ester-TPU/MWCNT nanocomposite and ester-TPUs as shown in Figure 5(b). These results indicate that the addition of MWCNTs increased the phase boundaries in ether- and ester-TPUs. The annealing process also promoted crystallization in ether- and ester-TPUs and their MWCNT nanocomposites, resulting in more phase boundaries.

The SAXS patterns of the TPU blend/MWCNT nanocomposites are shown in Figure 5(c). The inset figures in Figures 5(a)-(c) illustrate the values of $I_{(q)}\,q^2$ as a function of q obtained from the SAXS patterns. The Lorentz-correction, invariant quantity, Q_{inv} which describes the electron density fluctuation can be obtained by integrating $I_{(q)}\,q^2$ over the range of q as following eq. (1):

$$Q_{inv}=\int_0^\infty I_{(q)}q^2dq \tag{1}$$

Q_{inv} is known to adequately describe the electron density variation throughout the polymer and could be a criterion to judge the overall degree of phase separation.[2] Figure 6 illustrates Q_{inv} obtained from the SAXS data for ether- and ester-TPUs and TPU blends with and without MWCNTs. The Q_{inv} values of all the annealed samples are greater than those of the corresponding quenched samples. This is consistent with our previous results, which demonstrate that annealing promotes crystallization resulting in phase separation.

Comparing the Q_{inv} values of ether-TPUs and ester-TPUs, the ether-TPU samples showed higher Q_{inv} values than the ester-TPU samples, regardless of processing method and the presence of MWCNTs. This may be owing to the significant incompatibility between urethane hard segments and polyether soft segments, resulting in microphase separation in the case of the ether-TPU samples, whereas there is some degree of partial compatibility between urethane hard segments and polyester soft segments in the case of ester-TPUs.

In the ether-TPU and ester-TPU samples, the Q_{inv} values of samples with MWCNTs were higher than those without MWCNTs. Since MWCNTs appear to retard the phase separation between ether-TPUs and ester-TPUs as discussed in the above TEM analysis section, coagulation of the phase-separated domains is also retarded resulting in finely phase-separated structures with more phase boundaries, as shown in Figure 3(d). These additional phase boundaries lead to high Q_{inv} values.

In the literature, Li *et al*. proposed that MWCNTs may decrease the size of the dispersed phase in polycarbonate (PC)/polyethylene (PE)/MWCNT and ethylene vinyl acetate (EVA)/PE/MWCNT nanocomposites.[48] In the present study, MWCNTs are thought to interact with phenyl rings of both the ether and the ester hard segments through π-π interactions of phenyl rings of the hard segments and the MWCNTs. This may facilitate the mixing of hard segments of ether- and ester-TPUs, resulting in a decrease in the degree of phase separation in TPU blends. Consequently, the addition of MWCNTs

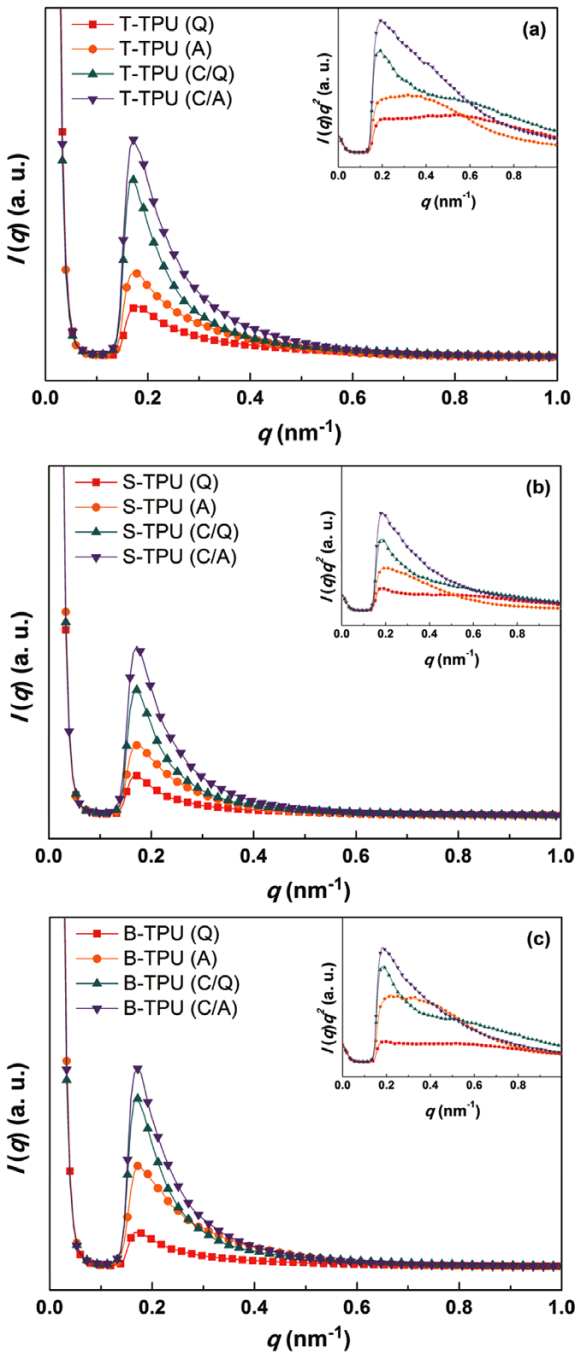

Figure 5. SAXS patterns of TPU/MWCNT nanocomposites containing: (a) ether-TPU, (b) ester-TPU, and (c) blend-TPU. The inset figures are values of $I_{(q)}\ q^2$ as a function of q obtained from SAXS patterns.

may lead to a retarding in the demixing of polyether and polyester soft segments. Another aspect is that, owing to the existence of MWCNTs in the co-continuous phase, the viscosity of the co-continuous phase increases to some extent, and this may also prevent coagulation of the domains as phase separation progresses, preventing the growth of the domain size.

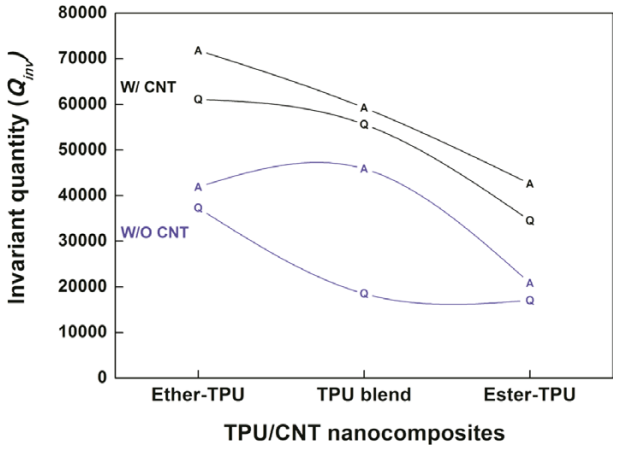

Figure 6. The invariant quantity (Q_{inv}) derived from SAXS data for TPU/MWCNT nanocomposites.

FTIR Analysis. Figure 7 shows the FTIR spectra of TPU blend/MWCNT nanocomposites containing 1 wt% MWCNT. In Figure 7(a), a N-H absorption peak is observed at approximately 3300 cm^{-1}, which is due to hydrogen-bonded N-H in the urethane linkage. Free N-H is observed as a very small shoulder at approximately 3400 cm^{-1}. N-H groups usually form hydrogen bonds with carbonyls (C=O) in the urethane linkage of the hard segment in ether- and ester-TPUs. The N-H groups are also capable of forming hydrogen bonds with ether oxygen (C-O-C) in the soft segment of ether-TPUs and with carbonyl (C=O) in the soft segment of ester-TPUs.

With the addition of MWCNTs, a reduction in the peak intensity of free N-H absorption at approximately 3412 cm^{-1} and a decrease in the frequency of the hydrogen-bonded N-H stretching vibration from 3312 to 3304 cm^{-1} are observed in Figure 7(a). These results indicate an increase in hydrogen bonding, especially between N-H and C=O carbonyls since the two N-H stretching vibrations at approximately 3312 and 3304 cm^{-1} are known to originate from the hydrogen bonding of N-H to ester oxygen and carbonyl, respectively.[49]

In Figure 7(b), carbonyl C=O absorption peaks are observed at 1730 and 1700 cm^{-1}, which are considered to be free and hydrogen-bonded carbonyls, respectively. In the spectra of the quenched and annealed TPU blend/MWCNT nanocomposites, the ratio of the intensity of the hydrogen-bonded C=O peak relative to that of the free C=O peak is observed to increase as compared to that of TPU blends without any MWCNTs. This increase indicates that the hydrogen bonding between N-H and carbonyls, whether they are in the hard segments or the soft segments of ester-based TPUs, increased by the addition of MWCNTs. This is consistent with the N-H peak analysis shown in Figure 7(a), and it means that MWCNTs cause an increase in the hydrogen bonding of the N-H of hard segments with the carbonyls of either soft or hard segments. This is also consistent with the SAXS analysis, which showed that TPUs with MWCNTs have more phase boundaries.

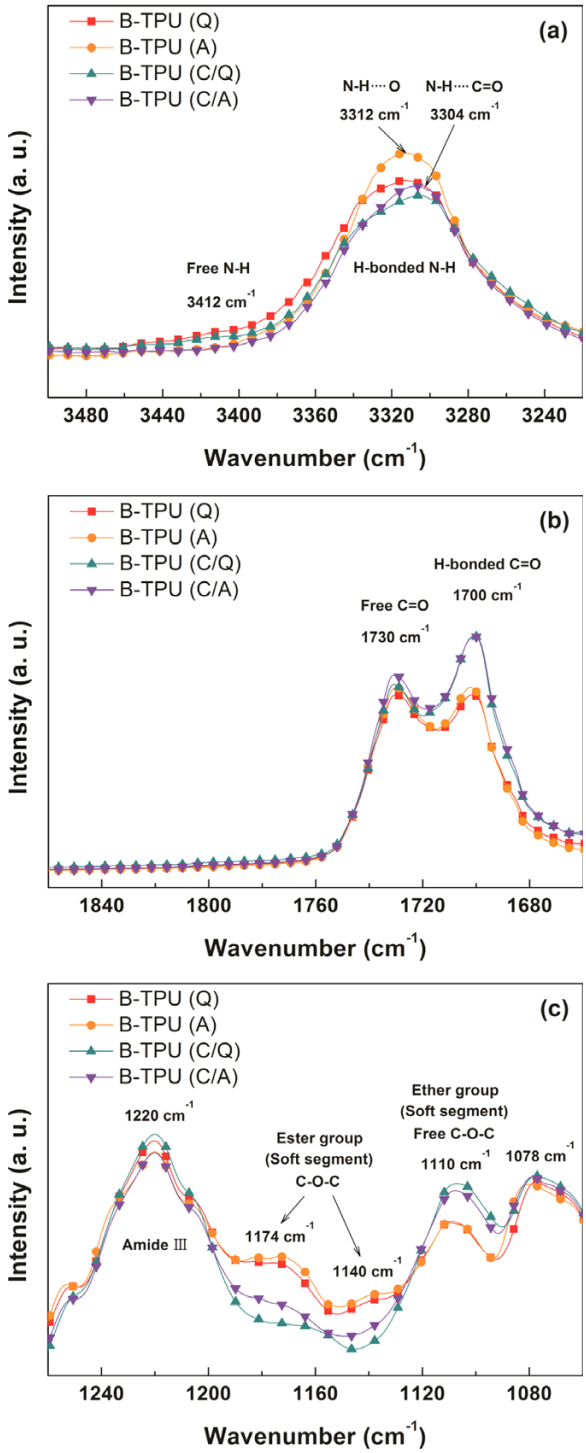

Figure 7. FTIR spectra covering (a) N-H, (b) C=O, and (c) C-O-C bands in TPU/MWCNT nano-composites.

Figure 7(c) shows the absorption peaks of the TPU blend/MWCNT nanocomposites in the 1260-1060 cm^{-1} region. It was previously reported that the absorptions at 1170 and 1140 cm^{-1} represent the C-O-C band in the ester group of the soft segment polyol of ester-TPUs.[50] The absorption corresponding to the C-O-C band of the soft segment polyol of ether-TPUs was reported to be at approximately 1110 and 1080 cm^{-1}.[51] When the absorption peaks of the TPU blend/MWCNT nanocomposites, either quenched or annealed, were compared to those of TPU blends without any MWCNTs, the TPU blend/MWCNT nanocomposites showed a decrease in the peak intensities of 1174 and 1140 cm^{-1} and an increase in that of 1110 cm^{-1}.

These results indicate that MWCNTs affect the environment of these C-O-C groups, perhaps owing to the forced mixing of ether and ester polyols by the simultaneous adsorption of hard-segment phenyl rings of ether-TPUs and ester-TPUs around MWCNTs. Since the soft segment polyol of ester-TPUs is more hydrophilic than that of ether-TPUs, the blending of two TPUs without any MWCNTs induced the phase separation between the two polyols, resulting in phase separation of the two TPUs. The addition of MWCNTs may reduce this kind of phase separation between the two kinds of polyols and thus retard the phase separation of ether- and ester-TPUs.

MWCNTs in the TPU blend seemed to not only to promote crystallization in the hard domains, resulting in an increase in the number of hydrogen bonds, they also retarded the phase separation of the two TPUs, resulting in microphase separation instead of macrophase separation. The morphology seen in the TEM pictures may be the result of those two effects. To better understand the nature of TPU blends and support the FTIR analysis on the morphology, the TPU/MWCNT nanocomposite samples were tested by DSC and DMA.

Results of DSC Analysis. Figures 8(a)-(c) show the DSC results obtained from the first heating cycle of the TPU/MWCNT nanocomposites prepared by quenching and annealing scanned from -150 to 250 °C. The ether-TPU samples shown in Figure 8(a) exhibit endothermic peaks at approximately 130 and 160 °C, corresponding to disruption of the short-range-domains and long-range-ordered hard domains, respectively. The endothermic peak at approximately 130 °C is assigned to the melting of the short-range-ordered crystallites formed during annealing. The endothermic peak at approximately 160 °C is assigned to the melting of hard-segment crystallites with long-range order, as reported in a previous study.[52] The ester-TPU samples shown in Figure 8(b) shows a high temperature peak at approximately 180 °C instead of 160 °C.

The areas under the endothermic peaks of ether-TPUs, ester-TPUs and TPU blends with or without MWCNTs depending on preparation method, quenching or annealing, are presented in Table II. The table shows that annealing increases the endothermic area or the amount of hard domains in all cases, as expected. Although the differences among endothermic areas are relatively small for all samples tested, some factors which may affect the results are discussed. For TPU samples without MWCNTs, the area under the endothermic peak of the quenched TPU blend (10.4 J/g) is smaller than that of ether-TPUs (12.1 J/g) or ester-TPUs (11.7 J/g). The same is also true for the TPU blend prepared by annealing. These results indicate that the addition of ether- or ester-TPUs in TPU blends

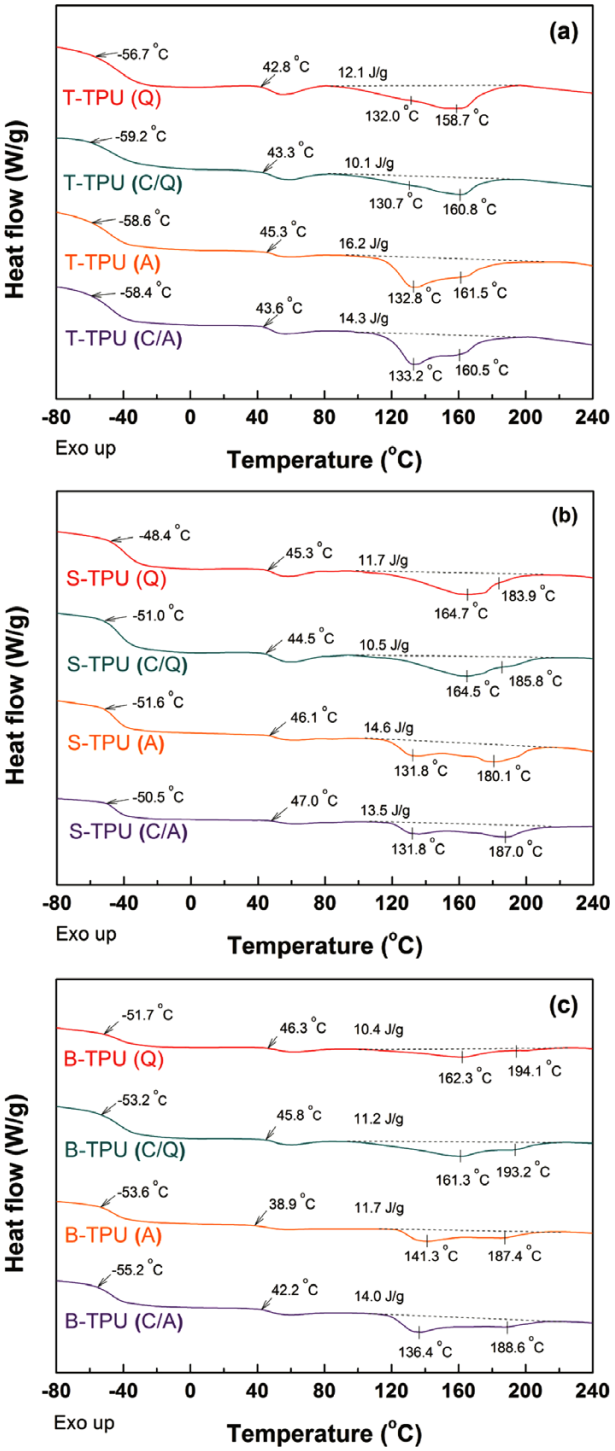

Figure 8. DSC thermograms of TPU/MWCNT nanocomposites of (a) T-TPUs, (b) S-TPUs, and (c) B-TPUs.

interferes with the ordering of hard domains of ether- or ester-TPUs, regardless of preparation method.

For TPU nanocomposites with MWCNTs, the amount of the hard domain or the ordering in the hard domain was observed to decrease by the addition of MWCNTs. The endothermic peak area of ether-TPUs with MWCNTs prepared by quenching (10.1 J/g) is smaller than that of ether-TPUs without MWCNTs (12.1 J/g). A similar trend was also observed for the ether-TPU/MWCNT nanocomposites prepared by annealing and for the ester-TPU/MWCNT nanocomposite samples prepared by quenching or annealing. Since area under the endothermic peaks may be related to the extent of crystallization of the hard domains, relative degree of crystallinity is obtained as follows; Areas under endothermic peaks of ether-TPU samples are divided by that of annealed ether-TPU (16.4 J/g) resulting in ratio of annealed ether-TPU to be unity. Ratios of ester-TPU samples are obtained compared to annealed ester-TPU (14.6 J/g). The medium value (15.4 J/g) between ether-TPU and ester-TPU is used as the reference one for blend TPUs. The resulting relative crystallinity values are shown in the parentheses in Table II.

Table II. Area Under the Endothermic Peak from the 1st Run DSC Results

Nanocomposites from Quenching	ΔH_m (J/g)	Nanocomposites from Annealing	ΔH_m (J/g)
T-TPU (Q)	12.1	T-TPU (A)	16.2
S-TPU (Q)	11.7	S-TPU (A)	14.6
B-TPU (Q)	10.4	B-TPU (A)	11.7
T-TPU (C/Q)	10.1	T-TPU (C/A)	14.3
S-TPU (C/Q)	10.5	S-TPU (C/A)	13.5
B-TPU (C/Q)	11.2	B-TPU (C/A)	14.0

For both the ether- and ester-based TPUs, MWCNTs appeared to decrease the crystallite formation in hard domains. This may be due to the interference of the MWCNTs in the molecular arrangement of urethane segments in the hard domains. Possible explanations may be the increase in the matrix viscosity by MWCNTs or the interference in urethane segment arrangement caused by the random adsorption of urethane segments on MWCNT surfaces.

For the TPU blend/MWCNT nanocomposites, it is interesting to note that the opposite trend was observed, as shown in Figure 8(c). The endothermic peak area of the quenched TPU blend/MWCNT nanocomposite (11.2 J/g) is larger than that of the quenched TPU blend without MWCNTs (10.4 J/g). The endothermic area of the annealed TPU blend/MWCNT nanocomposite (14.0 J/g) is much greater than that of the annealed TPU blend without MWCNTs (11.7 J/g). This means that MWCNTs increase the amount of hard domains in the case of the TPU blend. This is well correlated with the FTIR results, which showed that MWCNTs in the TPU blend appeared to promote crystallization in hard domains of TPU blends, resulting in an increase in hydrogen bonding. Some research exhibits that MWCNTs are expelled out of the crystalline phase into the amorphous phase[53] and increased crystallinity reduces the electrical conductivity of the composites.[54,55] The effect of crystallinity on the electrical resis-

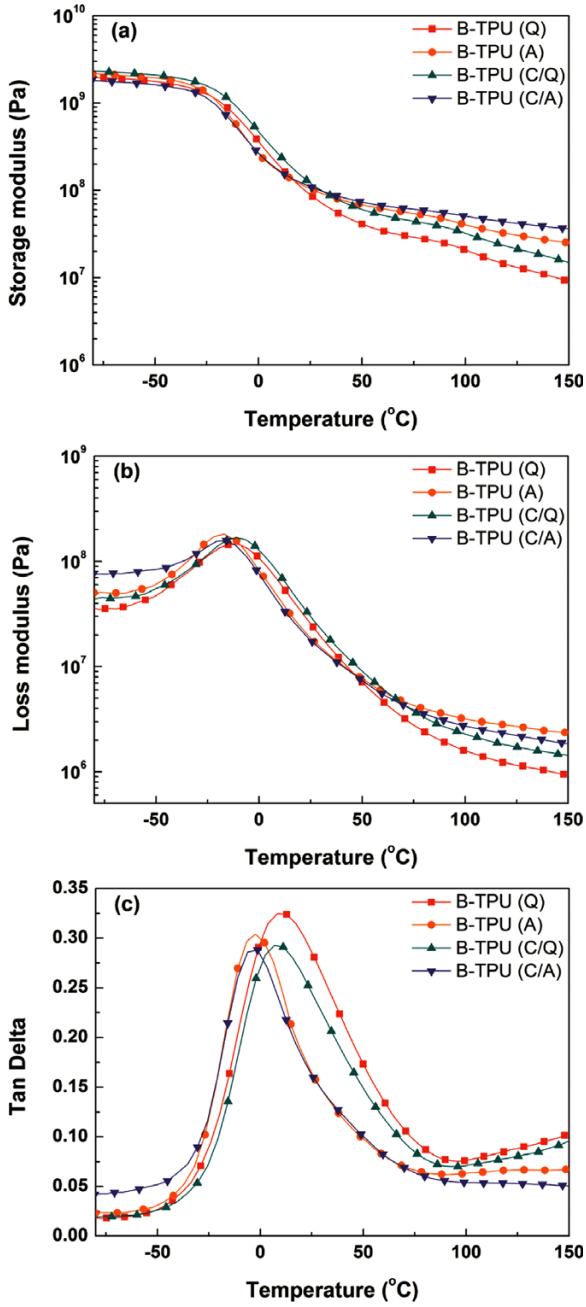

Figure 9. (a) Storage modulus, (b) loss modulus, and (c) tan delta versus temperature obtained from dynamic mechanical analysis measurement for TPU blend/MWCNT nanocomposites.

tivity of TPU containing MWCNTs is ambiguous and related study will be done in the future.

It is noted that the shape of melting peaks of annealed samples is different from that of quenched samples. Annealing appear to increase the area of lower endotherms around 130 °C, which indicates that annealing increase the crystallization of short range ordered soft segment domains.

Results of DMA Analysis. The dynamic mechanical properties of the TPU/MWCNT nanocomposites were measured to investigate the effect of the presence of MWCNTs on the temperature dependence of the dynamic mechanical properties. The storage modulus (E'), loss modulus (E'') and tan delta values of the quenched and annealed TPUs and TPUs/MWCNT nanocomposites are presented in Figure 9(a)-(c). The highest storage modulus is observed for the annealed TPU/blend/MWCNT nanocomposite, followed by the annealed TPU blend, the quenched TPU blend/MWCNT nanocomposite, and the quenched TPU blend. This order is exactly correlated with the order in the amount of endothermic area shown in Table II. This is as expected because the amount of endothermic area represents the amount of crystallites in the samples.

Regarding tan delta peak position temperatures, higher temperatures were measure for quenched blend samples than annealed samples. This is again consistent with the DSC results where higher glass transition temperatures were observed for quenched samples than annealed samples.

Conclusions

The electrical volume resistivity of the TPU/MWCNT nanocomposites were observed to vary depending on processing method, quenching or annealing, as well as on MWCNT loading. At 1.0 wt% MWCNT loading, the TPU blend/MWCNT nanocomposites based on ether-TPUs and ester-TPUs showed lower electrical resistivitiy (higher electrical conductivities) than either ether-TPU/MWCNT or ester-TPU/MWCNT nanocomposites.

TEM images showed the isolated droplet-type and co-continuous phase-separated morphologies for quenched and annealed TPU blend/MWCNT nanocomposites, respectively. These TEM results were shown to be consistent with the electrical volume resistivity results. The shifts in the G-band of the Raman spectra were shown to indicate interactions between the phenyl rings in the hard segments of TPUs and MWCNT. MWCNTs were better dispersed in the TPU blend/MWCNT nanocomposites than in either ether-TPUs or ester-TPUs. This is consistent with the electrical volume resistivity results.

Since SAXS provides information on phase-separated structures, the above TEM morphology was correlated with the electron density variations in the phase-separated system using the Lorentz-correction, Q_{inv}, in the SAXS analysis. From this analysis, the Q_{inv} values of samples with MWCNTs were observed to be higher than those without MWCNTs, indicating that MWCNTs may retard the phase separation.

Carbonyl, N-H, and C-O-C peaks in the FTIR spectra and the areas under the endothermic peaks of the TPU hard segments in DSC thermograms were analyzed to study changes in the morphology of the TPU blend/MWCNT nanocomposites. The macrophase mixing of ether-TPUs and ester-TPUs and supplementary hydrogen bonding between free carbonyl groups of the soft segments in ester-based TPUs and N-H in hard segments in ether-based TPUs were analyzed. DMA results were well correlated with the DSC results.

Acknowledgments. This study was supported by University of Suwon. The authors acknowledge the efforts of the Korea Basic Science Institute for taking nice TEM pictures.

References

(1) E. Unsal, B. Yalcin, I. Yilgor, E. Yilgor, and M. Cakmak, *Polymer*, **50**, 19 (2009).
(2) T. Thomson, *Polyurethanes as Specialty Chemicals*, CRC Press, Boca Raton, 2005.
(3) N. M. K. Lamba, K. A. Woodhouse, and S. L. Cooper, *Polyurethanes in Biomedical Applications*, CRC Press, Boca Raton, 1998.
(4) I. M. Pereira and R. L. Oréfice, *Macromol. Symp.*, **299/300**, 1 (2011).
(5) B. Fernández-d'Arlas, U. Khan, L. Rueda, J. N. Coleman, I. Mondragon, M. A. Corcuera, and A. Eceiza, *Compos. Sci. Technol.*, **71**, 8 (2011).
(6) E. Princi, S. Vicini, P. Stagnaro, and L. Conzatti, *Micron*, **42**, 1 (2011).
(7) C. H. Dan, M. H. Lee, Y. D. Kim, B. H. Min, and J. H. Kim, *Polymer*, **47**, 19 (2006).
(8) M. Arjmand, M. Mahmoodi, G. A. Gelves, S. Park, and U. Sundararaj, *Carbon*, **49**, 3430 (2011).
(9) M. Arjmand, M. Mahmoodi, S. Park, and U. Sundararaj, *J. Cell. Plast.*, **50**, 551 (2014).
(10) M. H. Al-Saleh and U. Sundararaj, *Macromol. Mater. Eng.*, **293**, 621 (2008).
(11) M. Arjmand, K. Chizari, B. Krause, P. Potschke, and U. Sundararaj, *Carbon*, **98**, 358 (2016).
(12) M. Arjmand and U. Sundararaj, *Compos. Sci. Technol.*, **118**, 257 (2015).
(13) M. Arjmand, A. Ameli, and U. Sundararaj, *Macromol. Mater. Eng.*, **301**, 555 (2016).
(14) E. Segal, R. Tchoudakov, M. Narkis, and A. Siegmann, *J. Polym. Sci., Part B: Polym. Phys.*, **41**, 1428 (2003).
(15) C. Zang, X. S. Yui, S. Asai, and M. Sumita, *Mater. Lett.*, **36**, 186 (1998).
(16) Y. Konishi and M. Cakmak, *Polymer*, **47**, 5371 (2006).
(17) J. Hong, D. W. Park, and S. E. Shim, *Macromol. Res.*, **20**, 465 (2012).
(18) B. D. Che, L. T. Nguyen, B. Q. Nguyen, H. T. Nguyen, T. Le, and N. H. Nguyen, *Macromol. Res.,* **22**, 1121 (2014).
(19) H. Koerner, W. Liu, M. Alexander, P. Mirau, H. Dowty, and R. A. Vaia, *Polymer*, **46**, 4405 (2005).
(20) J. Xiong, Z. Zheng, Xiumin Qin, M. Li, H. Li, and X. Wang, *Carbon*, **44**, 2701 (2006).
(21) H.-C. Kuan, C.-C. M. Ma, W.-P. Chang, S.-M. Yuen, H.-H. Wu, and T.-M. Lee, *Compos. Sci. Technol.*, **65**, 1703 (2005).
(22) I.-H. Kim, D. H. Baik, and Y. G. Jeong, *Macromol. Res.,* **20**, 920 (2012).
(23) B. S. Kim, S. H. Bae, Y.-H. Park, and J.-H. Kim, *Macromol. Res.,* **15**, 357 (2007).
(24) R. E. Gorga and R. E. Cohen, *J. Polym. Sci., Part B: Polym. Phys.*, **42**, 14 (2004).
(25) P. Zhao, K. Wang, H. Yang, Q. Zhang, R. Du, and Q. Fu, *Polymer*, **48**, 19 (2007).
(26) W. E. Dondero and R. E. Gorga, *J. Polym. Sci., Part B: Polym. Phys.*, **44**, 5 (2006).
(27) H. Ha, S. C. Kim, and K. Ha, *Macromol. Res.,* **18**, 660 (2010).
(28) S. Kim, J. W. Lee, I.-K. Hong, and S. Lee, *Macromol. Res.,* **22**, 154 (2014).
(29) G. Salimbeygi, K. Nasouri, A. M. Shoushtari, R. Malek, and F. Mazaheri, *Macromol. Res.,* **23**, 741 (2015).
(30) P. Potschke, A. R. Bhattacharyya, and A. Janke, *Carbon*, **42**, 965 (2004).
(31) P. Potschke, A. R. Bhattacharyya, and A. Janke, *Polymer*, **44**, 8061 (2003).
(32) M. Wu and L. L. Shaw, *J. Power Sources*, **136**, 37 (2004).
(33) R. A. Khare, A. R. Bhattacharyya, A. R. Kulkarni, M. Saroop, and A. Biswas, *J. Polym. Sci., Part B: Polym. Phys.*, **46**, 2286 (2008).
(34) M. Weber and M. R. Kamal, *Polym. Compos.*, **18**, 711 (1997).
(35) S. Abbasi, P. J. Carreau, and A. Derdouri, *Polymer*, **51**, 922 (2010).
(36) F. Jiang, G. Hu, S. Wu, Y. Wei, and L. Zhang, *Polym. Polym. Compos.*, **16**, 8 (2008).
(37) A. K. Barick and K. K. Tripathy, *Mater. Sci. Eng. B*, **176**, 18 (2011).
(38) M. F. Sonnenschein, Z. Lysenko, D. A. Brune, B. L. Wendt, and A. K. Schrock, *Polymer*, **46**, 23 (2005).
(39) H. D. Bao, Z. X. Guo, and J. Yu, *J. Polymer.*, **49**, 17 (2008).
(40) E. P. Favvas and A. C. Mitropoulos, *J. Eng. Sci. Technol. Rev.*, **1**, (2008).
(41) W. T. Chuang, U. S. Jeng, and H. S. Sheu, *Macromol Res.*, **14**, 1 (2006).
(42) M. Lee, H. Jeon, B. H. Min, and J. H. Kim, *J. Appl. Polym. Sci.*, **121**, 2 (2011).
(43) M. S. Dresselhaus, G. Dresselhaus, A. Jorio, A. G. Souza, and R. Saito, *Carbon*, **40**, 2043 (2002).
(44) F. Villalpando-Paez, A. Zamudio, A. L. Elias, H. Son, E. B. Barros, and S. G. Chou, *Chem. Phys. Lett.*, **424**, 345 (2006).
(45) S. Parnell, K. Min, and M. Cakmak, *Polymer*, **44**, 18 (2003).
(46) H. K. F. Cheng, T. Basu, N. G. Sahoo, L. Li, and S. H. Chan, *Polymers*, **4**, 2 (2012).
(47) H. Frielinghaus, N. Hermsdorf, R. Sigel, K. Almdal, K. Mortensen, I. W. Hamley, L. Messé, L. Corvazier, A. J. Ryan, D. V. Dusschoten, M. Wilhelm, G. Floudas, and G. Fytas, *Macromolecules*, **34**, 14 (2001).
(48) Z. M. Li, S. N. Li, X. B. Xu, and A. Lu, *Polym. Plast. Technol. Eng.*, **46**, 2 (2007).
(49) C. Zhang, J. Hu, S. Chen, and F. Ji, *J. Mol. Model.*, **16**, 8 (2010).
(50) J. G. Dillon and M. K. Hughes, *Biomaterials*, **13**, 4 (1992).
(51) S. B. Lin, K. S. Hwang, S. Y. Tsay, and S. L. Cooper, *Colloid Polym. Sci.*, **263**, 2 (1985).
(52) A. Frick and A. Rochman, *Polym. Test.*, **23**, 4 (2004).
(53) D. Bikiaris, *Materials*, **3**, 2884 (2010).
(54) N. Shukla and A. K. Thakur, *Ionics*, **15**, 357 (2009).
(55) A. Huegun, M. Fernandez, J. Pena, M. E. Munoz, and A. Santamaria, *Nanomaterials*, **3**, 173 (2013).